Anisotropic plasma crystal solitons

S. K. Zhdanov*
Moscow State Engineering and Physics Institute, Plasma Physics Department, Kashirskoe shosse 31, 115409 Moscow, Russia

D. Samsonov and G. E. Morfill
Max-Planck-Institut für Extraterrestrische Physik, D-85740 Garching, Germany
(Received 10 April 2002; published 26 August 2002)

An analytical two-dimensional model for weakly dispersive and weakly nonlinear longitudinal and transverse shear waves propagating in an ideal two-dimensional hexagonal Yukawa crystal is presented. The model takes into account the nonlinear terms up to the third order. Both compressional and shear soliton solutions are found in the long-wavelength approximation. It is shown that the compressional solitons are always supersonic and weakly anisotropic. The shear solitons, on the other hand, exhibit strong anisotropy and can be both subsonic and supersonic, depending on the direction of propagation. In the model, shear solitons cannot propagate along the main axes. The role of weak damping as well as formation of multiple solitons is analyzed. The results are discussed in connection with wave and Mach cone experiments in a monolayer hexagonal plasma crystal, and a diagnostic method is proposed to measure both the charge of the microparticles and the lattice parameter.

DOI: 10.1103/PhysRevE.66.026411 PACS number(s): 52.27.Lw, 05.45.Yv

I. INTRODUCTION

A soliton is an isolated wave that does not change its shape as it propagates. It was first observed by Robinson and Russel [1] on a water surface and described theoretically by Korteweg and de Vries [2]. Solitons are known to exist in plasmas and in various media such as viscous liquid films flowing on a vertical wall, rotating shallow fluids, planetary atmospheres, and magnetohydrodynamic systems [3]. Solitons are also known to propagate in crystalline solids [4].

Recently, the occurrence of solitons in dusty plasmas has been investigated. This has led to several important discoveries. Ion-acoustic solitons were studied theoretically [5] as well as experimentally [6]. Dust acoustic solitons in weakly coupled dusty plasmas were predicted in Ref. [7] and considered in a number of publications (see Ref. [8] and references therein). The most surprising discovery, however, was the realization that solitons can also exist in strongly coupled or even crystallized complex (dusty) plasmas. It was predicted in Ref. [9] that they can exist in a one-dimensional dust lattice, and finally compressional dust-lattice solitons were observed in a two-dimensional plasma crystal [10].

Plasma crystals can be created by adding micron-sized spherical particles to a plasma. The particles then collect ions and electrons. Since the electrons have higher mobility than the ions, the dust particles acquire a large negative charge (in the absence of electron emission from the grain surface) [11], and form one component of a ''complex plasma.'' Repelling particles are then confined by an external electric potential to form a cloud. When the particle potential energy exceeds its kinetic energy, the cloud becomes strongly coupled [12] and forms an ordered structure. In ground-based laboratory experiments, the dust particles are usually confined in the sheath region of a rf discharge [13–16] where the electric field is strong enough to levitate micron-sized spheres. This produces a two-dimensional complex plasma with only one or a few layers of particles.

It was suggested [17,18] that complex plasmas can be used as a classical model system for studying crystalline solids and microscopic phenomena therein such as wave propagation and phase transitions. The plasma crystals offer an advantage of being easily observed in real time with an ordinary video camera, unlike ''real'' solids.

Different wave modes can exist in plasma crystals. In a one-dimensional crystal, theory predicts compressional dust-lattice waves [9] and transverse vertical waves [19]. In a two-dimensional lattice, longitudinal (compressional) [20] and transverse shear [21] waves were studied experimentally. More complex wave structures (Mach cones or wakes) were also observed [22,23].

The theory predicts that as the wavelength gets shorter the lattice waves become more dispersive [24,25]. It is well known that a competition between the nonlinearity and dispersion of the waves can lead to the appearance of solitons. In this paper we report on an analytical theory that describes compressional and shear solitons in a monolayer hexagonal dust lattice.

II. THEORETICAL MODEL

The model is based on a set of equations of motion written for particles arranged in a monolayer hexagonal lattice (Fig. 1). We assume that the particles interact via a screened Coulomb (Yukawa) potential. This has proved to be a very good approximation [26,27] for the conditions of experiments we apply our theory to.

Particle spatial positions $\mathbf{r}_s$ are defined in our model by the following equation:

$$M(\ddot{\mathbf{r}}_s+\nu\dot{\mathbf{r}}_s)=\sum_{s'\neq s}\mathbf{F}_{s',s}+\mathbf{f}_s^{ext}, \tag{1}$$

*Email address: zh@plasma.mephi.ru

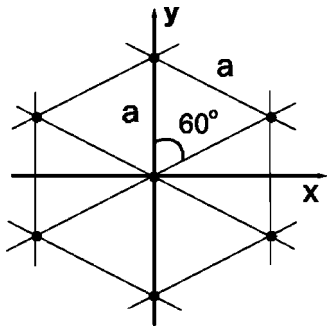

FIG. 1. Elementary hexagonal cell of a 2D lattice with the frame of reference used in this paper. Note that the coordinate system coincides with that of Ref. [21] and is orthogonal to that used in Ref. [25].

where M is the particle mass; ν is the damping rate due to the drag of the neutral gas; index $s=(n,m)$ denotes a pair of integer numbers n and m defining a site of a given particle in the unperturbed crystal (particle positions are $x_s=m\sqrt{3}a/2$, $y_s=a(n+m/2)$ for the coordinate system shown in Fig. 1); a is the particle separation; and $\mathbf{f}^{\text{ext}}$ is the external force exciting the wave. The interparticle force $\mathbf{F}_{s',s}$ can be expressed as

$$\mathbf{F}_{s',s}=-\nabla_{r_s}U_{s',s},\quad U_{s',s}=[Q^2/r_{s',s}]\exp(-r_{s',s}/\lambda_D),$$

$$r_{s',s}=|\mathbf{r}_{s'}-\mathbf{r}_s|,$$

where Q is the particle charge and λ_D is the Debye (screening) length. We considered Q and λ_D to be constant. The ratio a/λ_D is called the lattice parameter. It is an important parameter characterizing the properties of the plasma crystal.

In order to calculate the dispersion relations we assume that if the external force is small enough, the particle displacements $\mathbf{d}_s$ from the equilibrium positions $\mathbf{r}_s^0$ are small compared to the particle separation a. The particle positions are then $\mathbf{r}_s=\mathbf{r}_s^0+\mathbf{d}_s$ and we can expand the right-hand side of Eqs. (1) with respect to the amplitude of the displacement. Assuming further that the displacement is harmonic, that is $\mathbf{d}_s\sim\exp(-i\omega t+i\mathbf{k}\cdot r_s)$, one can find the dispersion relation in the form of $\omega=\omega(\mathbf{k})$ for the longitudinal and transverse waves that can sustain in the lattice. The result is shown in Fig. 2 for different angles θ between the X axis and the direction of propagation. In general, the dispersion relation is θ dependent and thus anisotropic. However, it becomes isotropic in the long-wavelength approximation (small k). In this case, the phonons can be considered as "purely" longitudinal (the displacement vector obeys the condition $\nabla\times\mathbf{d}=0$), or "purely" transverse ($\nabla\mathbf{d}=0$). This is true if the components of the dynamic matrix $\hat{W}$ [24,25] obey the condition

$$\frac{k_xk_y}{k^2}(W_{yy}-W_{xx})+W_{xy}\frac{k_x^2-k_y^2}{k^2}=0. \tag{2}$$

This condition is valid for any wavelength if the wave propagates along the X or Y directions shown in Fig. 1 or in the directions symmetric to them. It does not hold for an arbitrary angle of propagation and therefore the phonons are no longer purely longitudinal or purely transverse. This results in mixing of the longitudinal and transverse modes.

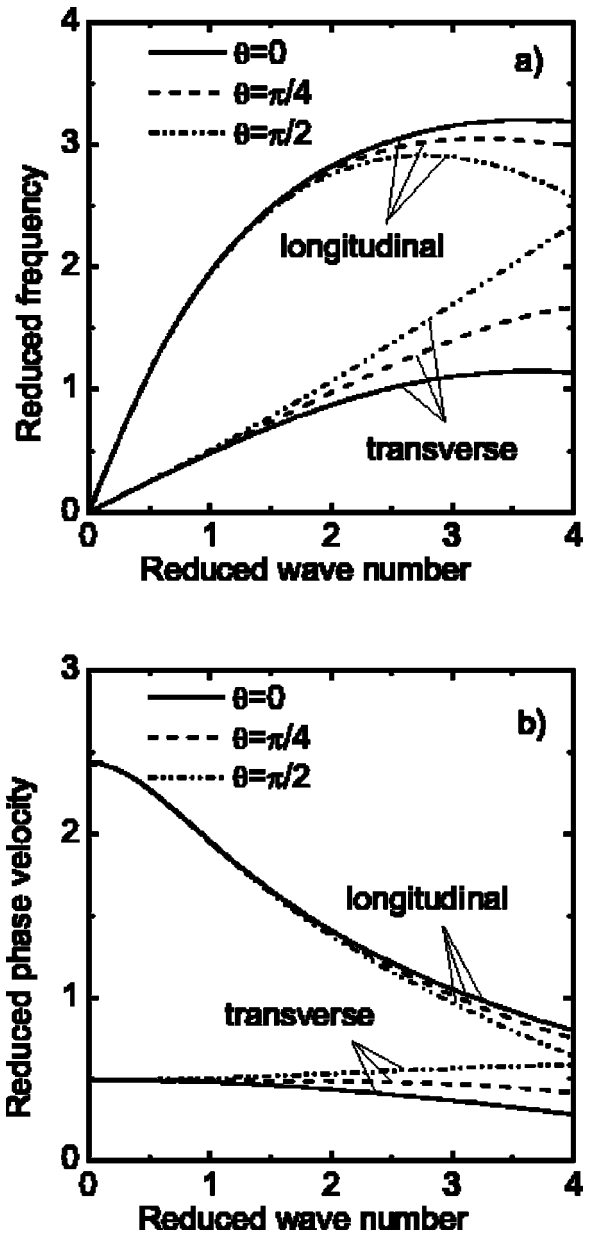

FIG. 2. Parameters of the longitudinal and transverse phonons versus the reduced wave number ka, for the angles of propagation $\theta=0$, $\pi/4$, and $\pi/2$, and for the lattice parameter $a/\lambda_D=1$. (a) Reduced phonon frequency, $\omega\sqrt{Ma^3}/Q$. (b) Reduced phonon phase velocity, $c\sqrt{Ma}/Q$, $c=\omega/k$. In the range of long wavelengths, the dispersion sign is always negative for longitudinal phonons, therefore, the phase velocity of these phonons always decreases when the wave number increases. For transverse phonons, the dispersion sign depends on the angle of propagation, and the phase velocities can increase or decrease with the wave number at different angles.

The dispersion relations obtained here are different from those of Ref. [24] because the former are calculated for real directions in the crystal while the latter are along the boundary of the first Brillouin zone. Since we will use these results to derive soliton solutions in the long-wavelength approxi-

TABLE I. Parameters of the long-wavelength linear dispersion relation (3) for longitudinal phonons for three values of the lattice parameter a/λ_D. c_l is the longitudinal dust-lattice wave speed normalized by $c_*=Q/\sqrt{Ma}$, l_l/a is the normalized dispersion length, and σ_l is the dispersion sign. c_l and σ_l are independent of the angle of propagation θ, whereas l_l has a weak dependence on θ. Note that X axis corresponds to $\theta=0$ and Y axis to $\theta=\pi/2$.

a/λ_D	θ	Any c_l/c_*	0 l_l/a	$\pi/2$ l_l/a	Any σ_l
0.5		3.632	1.483	1.483	−1
1		2.436	0.78	0.783	−1
2		1.517	0.436	0.446	−1

mation, it is worth mentioning that the calculated dispersion relations are linear for small k in the first approximation. We can represent the second-order dispersion corrections to this linear function as

$$\omega^2=c_1^2(1+\sigma_l l_l^2 k^2)k^2, \tag{3}$$

where c_l is the longitudinal dust-lattice wave speed, l_l is the dispersion length, and $\sigma_l=\pm 1$ is the sign of the dispersion correction. The same relation can be written for transverse waves with the indexes l replaced by tr. All these parameters are listed in Table I (longitudinal waves) and in Table II (transverse waves) for several values of the lattice parameter a/λ_D, which are in the range of known experiments [15,21–23,28]. The longitudinal dispersion length l_l significantly exceeds the transverse dispersion length l_{tr}. For the details of the calculations see Appendix.

The spectrum of longitudinal phonons is weakly anisotropic [25] and it has negative dispersion. This means that the phase velocity of these waves decreases when the wave number increases. In contrast, the spectrum of the transverse phonons is strongly anisotropic. Its dispersion sign changes with the direction of propagation.

III. LONG-WAVELENGTH SOLITONS ALONG THE MAIN AXES

The displacement vectors $\mathbf{d}_s$ appear in the dynamical Eqs. (1) only as differences at two fixed positions. At long wavelengths, one can use a Taylor expansion for these differences:

$$\begin{aligned}\mathbf{d}_{s'}-\mathbf{d}_s&=\delta x\partial_x\mathbf{d}+\delta y\partial_y\mathbf{d}+\tfrac{1}{2}(\delta x^2\partial_{xx}^2\mathbf{d}+2\delta x\delta y\partial_{xy}^2\mathbf{d}\\&\quad+\delta y^2\partial_{yy}^2\mathbf{d})+\cdots,\\ \delta x&\equiv x_{s'}^0-x_s^0,\quad \delta y\equiv y_{s'}^0-y_s^0,\quad x\equiv x_s^0,\quad y\equiv y_s^0,\end{aligned} \tag{4}$$

where $\mathbf{d}(x,y)$ is the displacement vector in the continuum limit.

As a result, we obtain a continuum model for a discrete crystal. If the particle displacements are distributed in space on a scale $\sim L$, then, obviously, the nth term of the series (4) is of the order of $(a/L)^n$, which is small in the continuum limit. Therefore, substituting Eq. (4) into Eqs. (1), and reexpanding the result with respect to the (small) displacement amplitude, one can obtain the dispersion relation in the linear long-wavelength approximation. It is found that this agrees with Ref. [24].

We can improve the linear theory, taking into account the finite amplitude of the displacements. In order to simplify the result, we treat the expansion as depending on two small parameters. The first parameter is the nonlinearity $d/a\ll 1$, the second is the dispersion $a/L\ll 1$. In other words, we omit the higher-order terms containing the products of these parameters.

If we consider a one-dimensional wave propagating along either the X axis (or along the Y axis) (Fig. 1), then the dynamic equations are

$$\begin{aligned}\partial_{tt}^2u+\nu\partial_t u&=\partial_{\eta\eta}^2\{c_{tr}^2(u-\sigma_{tr}l_{tr}^2\partial_{\eta\eta}^2u)\\&\quad+c_l^2(\Lambda_1uv+\tfrac{1}{2}\Lambda_3uv^2+\tfrac{1}{3}\Lambda_4u^3)+\cdots\},\\ \partial_{tt}^2v+\nu\partial_t v&=\partial_{\eta\eta}^2\{c_l^2(v+l_l^2\partial_{\eta\eta}^2v)+c_l^2(\tfrac{1}{2}\Lambda_1u^2+\tfrac{1}{2}\Lambda_2v^2\\&\quad+\tfrac{1}{2}\Lambda_3vu^2+\tfrac{1}{3}\Lambda_4v^3)+\cdots\},\end{aligned} \tag{5}$$

where η is the coordinate in the direction of the wave propagation; if the wave propagates along the X axis, then

$$\eta=x,\quad u=\partial_\eta d_y=\partial d_y/\partial x,\quad v=\partial_\eta d_x=\partial d_x/\partial x;$$

if the wave propagates along the Y axis, then

$$\eta=y,\quad u=\partial_\eta d_x=\partial d_x/\partial y,\quad v=\partial_\eta d_y=\partial d_y/\partial y,$$

where d_x and d_y are the components of the displacement vector $\mathbf{d}$. Indexes l and tr mark the parameters of the longitudinal and transverse waves, respectively; c is the phonon speed; σ is the sign of the dispersion; l is the dispersion length; Λ_{1-4} are the nonlinearity coefficients. The kinetic coefficients c_l, c_{tr}, σ_l, σ_{tr}, l_l, l_{tr}, and Λ_{1-4} are derived in the Appendix. The values of the nonlinearity coefficients are listed in Table III for several a/λ_D.

Note that Eqs. (5) correctly take into account all nonlinear terms up to the third order. Without the nonlinear terms, Eqs. (5) describe two independent phonons (compressional and shear). In the general case, Eqs. (5) are coupled, therefore propagation of a compressional wave can generate a weak

TABLE II. Parameters of the long-wavelength linear dispersion relation (3) for transverse phonons for three values of the lattice parameter a/λ_D. c_{tr} is the transverse dust-lattice wave speed normalized by $c_*=Q/\sqrt{Ma}$, l_{tr}/a is the normalized dispersion length, and σ_{tr} is the dispersion sign. c_{tr} is independent of the angle of propagation θ, whereas l_{tr} strongly depends on θ. The dispersion sign is opposite for the waves propagating along the main axes X ($\theta=0$) and Y ($\theta=\pi/2$).

a/λ_D	θ	Any c_{tr}/c_*	0 l_{tr}/a	$\pi/2$ l_{tr}/a	0 σ_{tr}	$\pi/2$ σ_{tr}
0.5		0.508	0.245	0.218	−1	+1
1		0.495	0.246	0.214	−1	+1
2		0.444	0.246	0.203	−1	+1

TABLE III. Nonlinearity coefficients of the dynamic equations (5) for three values of the lattice parameter a/λ_D and for waves propagating along the main axes X ($\theta=0$) and Y ($\theta=\pi/2$). Λ_1 and Λ_2 are the coefficients of the second-order nonlinearity, Λ_3 and Λ_4 are the coefficients of the third-order nonlinearity. The absolute values of all these coefficients increase with the lattice parameter.

		0	0	0	0	$\pi/2$	$\pi/2$	$\pi/2$	$\pi/2$
a/λ_D	θ	Λ_1	Λ_2	Λ_3	Λ_4	Λ_1	Λ_2	Λ_3	Λ_4
0.5		−0.114	−3.006	0.654	−0.269	0.054	−3.174	−0.572	0.235
1		−0.241	−3.024	1.402	−0.565	0.112	−3.373	−1.122	0.494
2		−0.518	−3.141	3.118	−1.175	0.213	−3.872	−2.419	1.019

shear, or a shear wave can produce a weak compression. However, this effect is small in the frame of the considered approximations.

It is interesting that a ''pure'' compressional wave is possible without excitation of any shear wave if a compressional disturbance propagate along one of the main axes (X or Y). In this case $u=0$ and neglecting the higher-order nonlinear terms we can simplify Eqs. (5) and obtain an equation for nonlinear compressional waves:

$$\partial_{tt}^2 v+\nu\partial_t v=\partial_{\eta\eta}^2\{c_l^2(v+l_l^2\partial_{\eta\eta}^2 v)+\tfrac{1}{2}\Lambda_2 c_l^2 v^2\}. \tag{6}$$

This equation has well-known solutions if the damping is neglected. Assuming a solution (with a small but finite amplitude A) in the form of a series,

$$v=A\sin\Theta+A^2\sin^2\Theta+\cdots,\quad \Theta=\omega t-k\eta, \tag{7}$$

one can easily obtain a nonlinear dispersion relation,

$$\omega^2=c_l^2k^2(1-k^2l_l^2+\tfrac{3}{4}\Lambda_2A^2). \tag{8}$$

Note that Λ_2 is always negative (Table III), so that the phase velocity of the nonlinear compressional wave has to diminish with increasing wave amplitude. This wave is stable against small modulations, as can be shown easily, using the well-known Lighthill criterion [29].

The solution corresponding to a compressional soliton is

$$v=A/\cosh^2(\Theta/L),\quad \Theta=\eta-ct,\quad L=2l_l/\sqrt{M^2-1},$$

$$AL^2=12l_l^2/\Lambda_2,\quad M=c/c_l, \tag{9}$$

where c is the soliton propagation speed. Note that the value of A is negative, so that the soliton amplitude is $|A|$.

Because $\Lambda_2<0$, we have negative v. This corresponds to a positive velocity of the particles moving in the wave,

$$V_x=\partial_t d_x=-c\partial_\eta d_x\equiv -cv=-Mc_lv>0,$$

for Mach numbers $M>0$. The particles move forward in the direction of the soliton propagation. This corresponds to an increase in the particle number density in agreement with the experimental observations [22,23,28].

Let us consider the shear waves. According to Eqs. (5) it is not possible to excite a ''pure'' shear wave without excitation of compression. However, since the compressional wave propagates faster than the shear wave of the same wavelength $[(c_l/c_{tr})^2\gg 1]$, we can consider the induced compression as quasistationary. This allows us to omit all time derivatives in the second equation of Eqs. (5), and to obtain an approximate relationship,

$$v+l_l^2\partial_{\eta\eta}^2 v\approx-\tfrac{1}{2}\Lambda_1u^2, \tag{10}$$

describing a stationary compression induced by a shear wave. Note that in the long-wavelength approximation, the second term on the left-hand side of this equation is small too. Omitting this term, one can find a very simple estimate for the amplitude of the induced compression,

$$v\approx-\tfrac{1}{2}\Lambda_1u^2. \tag{11}$$

Inserting this induced compression into Eq. (5) we obtain an equation that describes a nonlinear shear wave,

$$\partial_{tt}^2u+\nu\partial_t u=\partial_{\eta\eta}^2\{c_{tr}^2(u-\sigma_{tr}l_{tr}^2\partial_{\eta\eta}^2u)+\tfrac{1}{3}\tilde{\Lambda}_4c_l^2u^3\},$$

$$\tilde{\Lambda}_4=\Lambda_4-\tfrac{3}{2}\Lambda_1^2. \tag{12}$$

In contrast to Eq. (6), the nonlinear term is cubic. Besides, both the nonlinearity and dispersion are strongly anisotropic (see Appendix and Tables I, II, and III). It should be noted that the presence of the cubic nonlinearity in Eq. (12) favors generation of the third harmonic of the excited shear wave.

Substituting an expansion similar to Eq. (7) into Eq. (12), one can find a nonlinear dispersion relation (without damping) for the shear waves,

$$\omega^2=c_{tr}^2k^2(1+\sigma_{tr}k^2l_{tr}^2+\tfrac{1}{4}\tilde{\Lambda}_4[c_l/c_{tr}]^2A^2). \tag{13}$$

The nonlinearity coefficient Λ_4 is of the same order of magnitude as Λ_2 in Eq. (8) for the compressional wave, but now it is multiplied by a large factor $(c_l/c_{tr})^2\gg 1$. This makes the nonlinear effects more pronounced.

The shear waves are always stable [29] with respect to the modulational instability due to favorable combination of the signs of dispersion and nonlinearity in Eq. (12). As a consequence, however, there are no shear soliton solutions in the long-wavelength approximation.

IV. SOLITONS PROPAGATING IN AN ARBITRARY DIRECTION

If the wave propagates in an arbitrary direction, the continuum model becomes very complicated due to the anisotropy and is not considered here. We derive the anisotropic

two-dimensional dynamic equations describing the solitary waves, starting from Eq. (1), using the procedure analogous to that employed for deriving Eq. (5) and then substituting the new independent variables,

$$\Theta = ct - x\cos\theta - y\sin\theta, \quad k_x = k\cos\theta, \quad k_y = k\sin\theta, \tag{14}$$

where θ is the angle between the wave vector and the X axis and c is the soliton velocity. The particular cases of $\theta = 0$ (X direction) and $\theta = \pi/2$ (Y direction) were already considered in Sec. III.

The derived equations are analogous to Eq. (5) but significantly more complicated. We do not write them down here to save space and proceed with further analysis. In these equations, we substitute new variables R and D which satisfy the relations,

$$\partial_\Theta d_x = -D\cos\theta - R\sin\theta, \quad \partial_\Theta d_y = R\cos\theta - D\sin\theta. \tag{15}$$

Then the resulting equations, which describe solitons propagating in an arbitrary direction, can be written in the form

$$\begin{aligned}(c^2 - c_l^2)D = c_l^2[l_l^2(\theta)D'' + \tfrac{1}{2}\{\Lambda_2(\theta)D^2 + \Lambda_1(\theta)R^2\} \\ + \Lambda_5(\theta)RD] - \sigma_{cr}(\theta)c_{tr}^2 l_{cr}^2(\theta)R'', \\ (c^2 - c_{tr}^2)R = -c_{tr}^2[\sigma_{tr}(\theta)l_{tr}^2(\theta)R'' + \sigma_{cr}(\theta)l_{cr}^2(\theta)D''] \\ + c_l^2[\tfrac{1}{2}\Lambda_5(\theta)(D^2 - R^2) + \Lambda_1(\theta)RD].\end{aligned} \tag{16}$$

Here, c_l, and c_{tr} are the above-introduced ''sound'' speeds for compressional and shear waves, respectively; $l_l(\theta)$ and $l_{tr}(\theta)$ are the dispersion lengths for the longitudinal and transverse waves [analogous to those introduced in Eqs. (5)]; $l_{cr}(\theta)$ is the dispersion length defining the nondiagonal component of the dispersion matrix; $\sigma_{tr}(\theta)$, and $\sigma_{cr}(\theta)$ are the corresponding dispersion signs; $\Lambda_1(\theta)$, $\Lambda_2(\theta)$, and $\Lambda_5(\theta)$ are the coefficients of the second-order nonlinearity (all terms of higher order are neglected); primes denote derivatives with respect to Θ. These coefficients are shown in Fig. (3). It should be noted that they are, of course, periodic functions of the angle θ (with a period of $\pi/3$) and thus we need only consider the interval $0 \leqslant \theta \leqslant \pi/3$. (Due to the hexagonal symmetry of the lattice, the conditions of propagation, for example, at $\theta = \pi/6$ along the X axis are equivalent to those at $\theta = \pi/2$ along the Y axis.)

The dispersion signs are defined as

$$\sigma_{cr}(\theta) = \begin{cases} -1, & 0 \leqslant \theta \leqslant \pi/6, \\ +1, & \pi/6 \leqslant \theta \leqslant \pi/3, \end{cases}$$

$$\sigma_{tr}(\theta) = \begin{cases} -1, & 0 \leqslant \theta \leqslant \theta_*, \ \pi/3 - \theta_* \leqslant \theta \leqslant \pi/3, \\ +1, & \theta_* \leqslant \theta \leqslant \pi/3 - \theta_*, \end{cases} \tag{17}$$

where θ_* is the critical angle at which the transverse dispersion changes the sign (see Fig. 3).

At critical points where the dispersion signs $\sigma_{tr}(\theta)$ and $\sigma_{cr}(\theta)$ change, the corresponding dispersion lengths $l_{tr}(\theta)$, and $l_{cr}(\theta)$ are equal to zero. This means that at these particular points the dispersion corrections of the next order should be taken into account and the discussed theory is not valid. It is also interesting that the parameters $l_l(\theta)$, $\Lambda_1(\theta)$, and $\Lambda_2(\theta)$ change monotonically in the half-period interval, $0 \leqslant \theta \leqslant \pi/6$, whereas $\Lambda_5(\theta)$ does not.

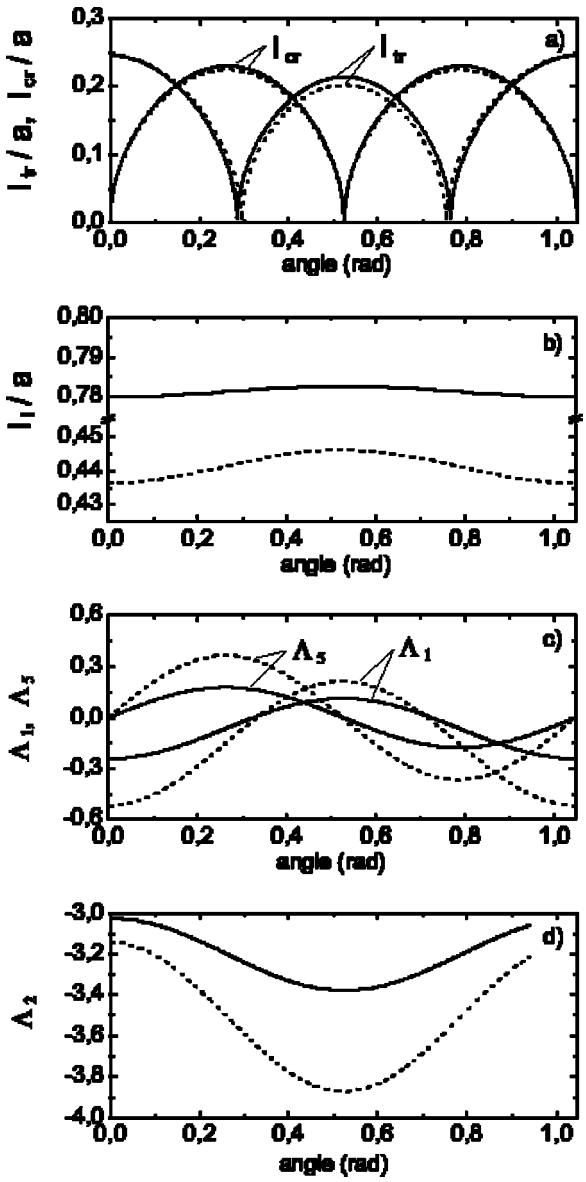

FIG. 3. Angular dependence of the kinetic coefficients of Eqs. (16) for two values of the lattice parameter $a/\lambda_D = 1$ (solid line), and $a/\lambda_D = 2$ (dashed line). (a) Transverse l_{tr} and cross l_{cr} dispersion lengths. They are weak functions of the lattice parameter, but vary significantly with the angle. The transverse dispersion length is equal to zero (transverse dispersion changes sign) at $\theta = 0.284$, for $a/\lambda_D = 1$, and at $\theta = 0.294$, for $a/\lambda_D = 2$. (b) Longitudinal dispersion length l_l. It has a weak dependence on the angle, but strongly changes with the lattice parameter. (c) Nonlinearity coefficients Λ_1, Λ_5. (d) Nonlinearity coefficient Λ_2.

Simplified particular solutions of Eqs. (16) can be found taking into account the fact that the inequality $(c_l/c_{tr})^2 \gg 1$ is valid for the values of the lattice parameter a/λ_D for

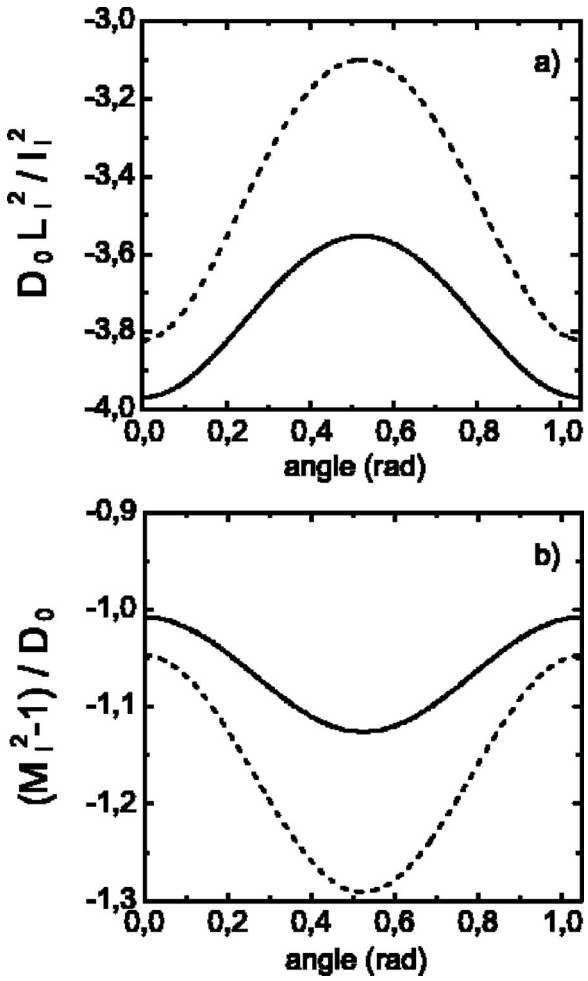

FIG. 4. Parameters of the compressional soliton (19) versus the angle of propagation for two values of the lattice parameter $a/\lambda_D = 1$ (solid line) and $a/\lambda_D = 2$ (dashed line). (a) Soliton parameter $D_0 L_l^2$ normalized by the longitudinal dispersion length l_l, (b) soliton velocity parameter $(M_l^2-1)/D_0$.

known experiments. It was measured experimentally that $c_l \simeq 20$ mm/s [23], and $c_{tr} \simeq 6$ mm/s [21], so that $(c_l/c_{tr})^2_{\rm exp} \simeq 10 \gg 1$. These measurements agree with the estimates listed in Tables I and II.

Since $(c_l/c_{tr})^2 \gg 1$, we can speak of a compressional soliton accompanied by a small shear, or a shear soliton accompanied by a small compression as considered above for propagation along the main axes X ($\theta = 0$) and Y ($\theta = \pi/2$). The compressional soliton, being faster, must obey the equation obtained from Eqs. (16),

$$(c^2 - c_l^2) D = c_l^2 l_l^2(\theta) D'' + \tfrac{1}{2} c_l^2 \Lambda_2(\theta) D^2, \tag{18}$$

whereas the induced shear can be roughly estimated as $R \sim \Lambda_5(\theta) D^2/2$.

The compressional soliton solution can be easily obtained,

$$D = D_0(\theta)/\cosh^2(\Theta/L_l(\theta)), \quad \Theta = ct - x\cos\theta - y\sin\theta, \tag{19}$$

where the soliton amplitude $D_0(\theta)$ and the soliton width $L_l(\theta)$ are defined by

$$D_0(\theta)[L_l(\theta)/l_l(\theta)]^2 = 12/\Lambda_2(\theta),$$
$$(M_l^2 - 1)[L_l(\theta)/l_l(\theta)]^2 = 4, \quad M_l \equiv c/c_l. \tag{20}$$

Figure 4 shows the angular dependence of these parameters.

The first relation of Eqs. (20) can be simplified for the case $0.5 \leqslant a/\lambda_D \leqslant 2$, which is a useful approximation for many experiments,

$$|D_0| L_l^2 \cong 1.97 \lambda_D^2 [1 + p(\theta) a/\lambda_D], \tag{21}$$

where $p(\theta)$ is a small anisotropy factor that varies in the interval $p(\pi/2) \leqslant p(\theta) \leqslant p(0)$ where $p(\pi/2) = 0.108$ and $p(0) = 0.224$. Equation (21) is also valid in case of weak damping and a weakly inhomogeneous crystal layer.

The soliton amplitude $D_0(\theta)$ is negative at all angles of propagation because $\Lambda_2(\theta) < 0$. But the velocity component normal to the soliton front and the variation in the particle number density are always positive:

$$V_N = -cD = -M_l c_l D > 0, \quad \delta n/n = V_N/c = -D > 0,$$
$$\mathbf{N} = \mathbf{k}/k. \tag{22}$$

Since the compressional soliton is always supersonic ($M_l > 1$), it is stable against perturbations not changing its symmetry. Being faster the soliton can run away from the perturbations. On the other hand, the soliton can generate sound, for example, due to inhomogeneity of the real crystal. This can be an effective damping mechanism. The stability conditions against transverse perturbations have to be studied separately.

The shear soliton, which is slower than the compressional, obeys the equation

$$(c_{tr}^2 - c^2) R = \sigma_{tr}(\theta) c_{tr}^2 l_{tr}^2(\theta) R'' + \tfrac{1}{2} c_l^2 \Lambda_5(\theta) R^2. \tag{23}$$

Note that at $\theta = 0, \pi/2$ the nonlinearity coefficient becomes zero and the equation has no soliton solutions. The small compression induced by the shear soliton can be estimated using the equation

$$l_l^2(\theta) D'' + D \cong -\tfrac{1}{2} \Lambda_1(\theta) R^2. \tag{24}$$

If the soliton width is much greater than the longitudinal dispersion length, then the first term on the left-hand side of this equation is negligible, and we can use the estimate (11). In the long-wavelength approximation this term can be treated as a small correction.

A solution of Eq. (23) describing the shear soliton is similar to that describing the compressional soliton (19),

$$R = R_0(\theta)/\cosh^2[\Theta/L_{tr}(\theta)]. \tag{25}$$

Both the amplitude and the width of this solution are defined now by

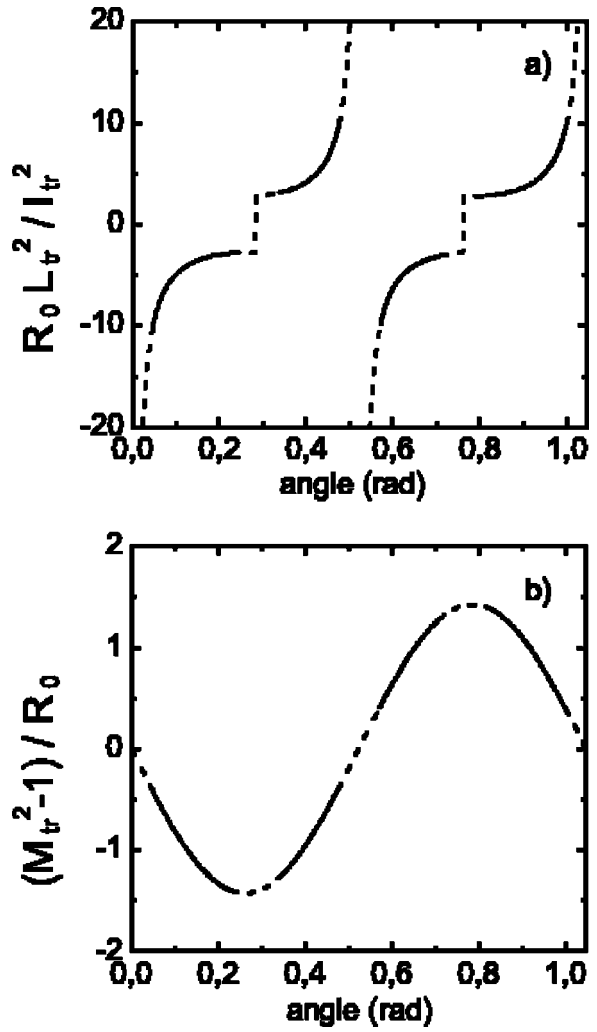

FIG. 5. Parameters of the shear soliton (25) versus the angle of propagation, for $a/\lambda_D=1$. (a) Soliton parameter $R_0 L_{tr}^2$ normalized by the longitudinal dispersion length l_{tr}; (b) soliton velocity parameter $(M_{tr}^2-1)/R_0$. Dotted lines show the regions where the theory considered here is not valid. The soliton parameter and the soliton velocity parameter have very little dependence on the lattice parameter in the range $1<a/\lambda_D<2$.

$$R_0(\theta)[L_{tr}(\theta)/l_{tr}(\theta)]^2=[12\sigma_{tr}(\theta)/\Lambda_5(\theta)](c_{tr}/c_l)^2,$$
$$(M_{tr}^2-1)[L_{tr}(\theta)/l_{tr}(\theta)]^2=-4\sigma_{tr}(\theta), \quad M_{tr}\equiv c/c_{tr}. \tag{26}$$

Figure 5 shows the angular dependence of these parameters.

We should point it out that our approximation is not valid near the points marked in Fig. 5 with dashed lines, where the dispersion length l_{tr} or the nonlinear coefficient Λ_5 becomes very small. This agrees with our previous result that there are no shear soliton solutions propagating along the main axes X and Y. In order to construct a theory valid in these regions, one has to calculate the higher-order dispersion corrections and nonlinear coefficients, which is a very tedious problem. The long-wavelength approximation cannot be used in this case.

Note that according to Eqs. (26), the shear soliton has to be supersonic in the regions of the negative transverse dispersion [determined above by Eqs. (17)], and it has to be subsonic in the regions of the positive dispersion. In the latter case, the shear soliton might become unstable.

Surprisingly, the parameters of the shear soliton have only a very weak dependence on the value of the lattice parameter if $1<a/\lambda_D<2$.

V. GENERATION OF MULTISOLITON STRUCTURES

So far we considered only single soliton solutions. However, if the perturbation is energetic enough it can generate several solitons. We estimate the number of solitons using the associated Schrödinger equation [4,30] and assuming that the amplitude of all the solitons is small. In that case the solitons propagate almost with the acoustic velocity of the phonons constituting this wave packet. Since the difference between the soliton and the phonon speeds is small, we can further simplify our model.

For compressional waves we can rewrite Eq. (6) in the frame of reference moving with the longitudinal phonon. Omitting the damping we obtain

$$\partial_t U+U\partial_\eta U+\tfrac{1}{2}c_l l_l^2\partial_{\eta\eta\eta}^3 U=0, \quad U\equiv\tfrac{1}{2}\Lambda_2 c_l v. \tag{27}$$

This equation is the well-known Korteweg–de Vries (KdV) equation and we can use all the methods developed for its analysis.

Following the qualitative approach proposed in Ref. [31], let us introduce a parameter

$$P=\frac{|U_0|L^2}{6c_l l_l^2}, \tag{28}$$

where U_0 is the amplitude, and L is the spatial scale of the perturbation. Because the parameter P is directly proportional to the amplitude of the perturbation, it characterizes the nonlinearity of the initial perturbation. Note that this parameter identically equals unity for a single soliton.

The value of P determines the number of solitons that can be produced by the given initial perturbation. It was shown in Ref. [31] that if $P<1$, then no more than a single soliton can be produced. If $P\gg 1$ many solitons can appear, and the number of the solitons can be estimated as $N\sim P^{1/2}$.

In our case, Eq. (28) can be rewritten in the more convenient form,

$$P=\frac{|\Lambda_2|}{12}\left(\frac{L}{l_l}\right)^2\frac{\delta n}{n}, \tag{29}$$

which can be used for quantitative estimates.

We can estimate the value of P for the experiments of Ref. [10]. Substituting the measured parameters, i.e., the number density variation $\delta n/n=0.3-0.4$, the soliton width $L=2-2.5$ mm, the lattice parameter $a/\lambda_D\simeq 1$ into Eq. (29), and using the parameters estimated in Tables I, II, i.e., $|\Lambda_2|\simeq 3$, $l_l\simeq 0.5$ mm, we obtain $P=1.2-1.5$. This value means that about 1–2 well-resolved solitons should be observed. Two solitons, one strong and one weak were indeed observed in these experiments.

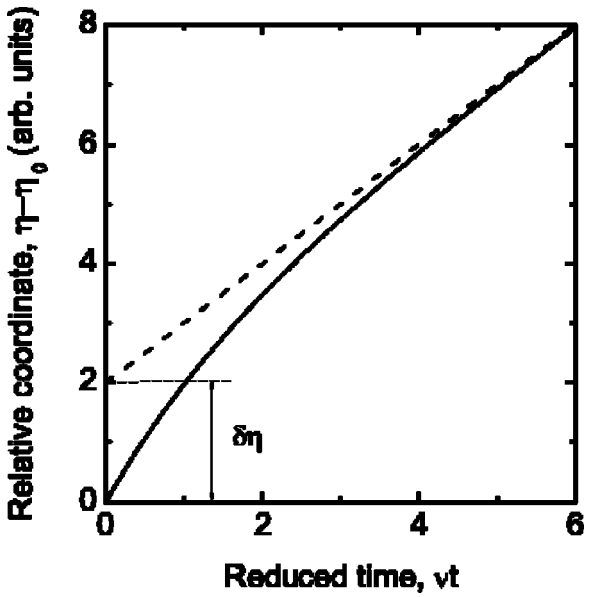

FIG. 6. Trajectory of a damped compressional soliton versus propagation time. The soliton was generated at $t=0$. The asymptote to the soliton trajectory (dashed line) has a slope proportional to the dust-lattice wave speed c_l. Its offset $\delta\eta$ can be used to determine the damping rate.

VI. ROLE OF DAMPING

The analytical soliton solutions Eqs. (9), (19), and (25) were obtained without damping. In case of weak damping, when the soliton width is much smaller than the damping length, these solutions are locally valid. However, the amplitude and the width will not be constant as the soliton propagates. Here we calculate how these parameters change with time.

The spatial scale of damping can be estimated as $L_{\mathrm{damp}} \sim c/\nu$, where c is the wave velocity and ν is the damping rate. Therefore, slower waves have shorter damping length. Since the shear wave has smaller velocity than the compressional, the damping affects it stronger.

Let us consider the case of a compressional soliton (9), but now taking into account weak damping. We introduce a new variable "flow potential" ψ, defined as $v=\partial_\eta\psi$ and rewrite Eq. (6) as

$$\partial_{tt}^2\psi+\nu\partial_t\psi=\partial_\eta\{c_l^2(v+l_l^2\partial_{\eta\eta}^2 v)+\tfrac{1}{2}\Lambda_2 c_l^2 v^2\}. \qquad (30)$$

This form makes it easy to prove that for any solution vanishing at infinity ($v\to 0$, when $\eta\to\pm\infty$), the following relations are true:

$$\partial_t H=-\nu I,$$

$$H\equiv\int_{-\infty}^{\infty} d\eta\left\{\frac{1}{2}[c_l^{-2}(\partial_t\psi)^2+v^2-l_l^2(\partial_\eta v)^2]+\frac{\Lambda_2}{6}v^3\right\}, \qquad (31)$$

$$I\equiv\int_{-\infty}^{\infty} d\eta c_l^{-2}(\partial_t\psi)^2.$$

TABLE IV. Comparison of the normalized soliton parameter $|A|L^2/a^2$ calculated using the two-dimensional model (5) for compressional solitons propagating along the X axis ($\theta=0$) and Y axis ($\theta=\pi/2$), with the linear chain models, taking into account interaction only with the nearest neighbors and with all neighbors. The anisotropy accounts for 5–20% difference in the soliton parameters. The linear chain model with all neighbors differs by a factor of 1.5–2.7 and can be used for rough estimates. The linear chain model with nearest neighbors differs by an order of magnitude and can be used only for $a/\lambda_D \gg 1$.

a/λ_D	Hexagonal, $\theta=0$	Hexagonal, $\theta=\pi/2$	Chain, all neighbors	Chain, nearest neighbors
0.5	8.779	8.315	3.155	0.329
1	2.414	2.181	1.076	0.313
2	0.726	0.616	0.414	0.263

These relations correspond to wave energy conservation-the energy H of any compact wave packet diminishes in time under the action of damping. For the soliton (9), all parameters in these relations can be found analytically:

$$H=\frac{4M^2+1}{5}W,\quad I=M^2W,\quad W=\int_{-\infty}^{\infty} d\eta v^2=\frac{4}{3}A^2L,$$

$$M\equiv\frac{c}{c_l}, \qquad (32)$$

where W is the soliton wave energy [31], A is the soliton amplitude, and M is the soliton Mach number.

If the soliton has a small amplitude, then $M\approx 1$ and as a consequence $H\approx W$. In this case the wave energy diminishes exponentially,

$$\frac{dW}{dt}=-\nu W,\quad W=W_0\exp(-\nu t), \qquad (33)$$

where W_0 is the initial energy (at the moment of the soliton formation). The soliton width L, amplitude A, and Mach number M scale as

$$L\sim W^{-1/3},\quad |A|\sim W^{2/3},\quad M-1\sim W^{2/3}, \qquad (34)$$

and their time dependence is

$$L=L_0\exp(\nu t/3),\quad A=A_0\exp(-2\nu t/3),$$

$$M-1=(M_0-1)\exp(-2\nu t/3), \qquad (35)$$

where the index 0 marks the initial values.

Now we can improve our estimate of the damping length for the soliton amplitude:

$$L_{\mathrm{damp}}\approx 1.5c/\nu. \qquad (36)$$

In case of no damping the soliton propagates with a constant velocity, whereas according to Eqs. (35) the soliton gradually decelerates under the action of damping. The resulting trajectory of the soliton is

TABLE V. Comparison of the normalized longitudinal dust-lattice wave speed $c_l\sqrt{Ma/|Q|}$ calculated using the two-dimensional model (5) for compressional solitons propagating along the X axis ($\theta=0$), and Y axis ($\theta=\pi/2$), with the linear chain models, taking into account interaction only with the nearest neighbors and with all neighbors. The dust-lattice wave speed is isotropic in the long-wavelength approximation. The linear chain model with all neighbors differs by a factor of 1.2–1.7 and can be used for most estimates. The linear chain model with the nearest neighbors differs more, by a factor of 1.3–2.7, but it can also be used for rough estimates even for $a/\lambda_D \lesssim 1$.

a/λ_D	Hexagonal, $\theta=0$	Hexagonal, $\theta=\pi/2$	Chain, all neighbors	Chain, nearest neighbors
0.5	3.632	3.632	2.094	1.404
1	2.436	2.436	1.733	1.356
2	1.517	1.517	1.281	1.163

$$\eta-\eta_0=c_l t+\frac{3}{2}\frac{c_0-c_l}{\nu}[1-\exp(-2\nu t/3)]. \tag{37}$$

This is shown qualitatively in Fig. 6. At the initial stage, the slope of the trajectory is determined by the initial soliton velocity c_0. Then the slope of the trajectory diminishes, due to the decrease in the soliton velocity. At the final stage the soliton propagates with a constant velocity, which is equal to the propagation speed of the corresponding phonon. The soliton trajectory has an offset,

$$\delta\eta=\frac{3}{2}\frac{c_0-c_l}{\nu}. \tag{38}$$

If the damping is too strong, the soliton will be damped before it forms, and then no solitons can be observed. This can happen if the damping time $1/\nu$ is shorter than the soliton generation time scale δt, which is

$$\delta t\propto\frac{l_l}{2c_l}\left(\frac{6c_l}{U_0}\right)^{3/2}\propto\frac{l_l}{2c_l P^{3/2}}\left(\frac{L}{l_l}\right)^3, \tag{39}$$

where P is defined by Eq. (28). Comparing this time scale with the damping time, one can obtain a criterion,

$$\nu<\nu_{cr},\quad \nu_{cr}=\frac{3c_l}{l_l}\left(\frac{|\Lambda_2|}{12}\frac{\delta n}{n}\right)^{3/2}, \tag{40}$$

defining the critical damping.

For the experiments of Ref. [10], we have $c_l=20-30$ mm/s, $\delta n/n=0.4$. The resulting critical damping is $\nu_{cr}=3.5-5\ \mathrm{s}^{-1}$. The damping due to the neutral drag was $\nu=2.5\ \mathrm{s}^{-1}$, lower than the critical damping.

VII. DISCUSSION AND APPLICATION TO EXPERIMENT

In the experiments of Ref. [10], it was found that the soliton parameter $|A|L^2$ is approximately constant as the soliton propagates. As the amplitude $|A|$ decreased due to damping, the width L increased accordingly. Even though the linear chain model, used in Ref. [10] to interpret the measurements, provided a very good qualitative explanation, we found that its quantitative results disagreed by a factor of about 2.

Using the two-dimensional model (5), we calculated the soliton parameter $|A|L^2$ (Table IV) and the longitudinal dust-lattice wave speed c_l (Table V), and compared them to the results obtained with the linear chain model. Whilst the anisotropy accounts for less than 20% difference in the soliton parameter, the linear chain model (taking into account all neighbors) is substantially different, by a factor of 1.5–2.7, and can be used only for rough estimates. The linear chain model with only nearest neighbors differs by about an order of magnitude and should not be used. The longitudinal dust-lattice wave speed is less sensitive to the model choice. Both linear chain models provide an error of less than a factor of 2.7.

Even though the experiments of Ref. [10] were conducted in a two-dimensional lattice, an anisotropy was not reported. A possible reason is that the compressional solitons are weakly anisotropic with less than 20% difference in both soliton parameter and velocity (Fig. 4). Only precise measurements using a perfect lattice with well-controlled orientation can detect this difference. On the other hand, the shear solitons are strongly anisotropic. Their soliton parameter and velocity vary by more that a factor of 3 (Fig. 5), and in addition, they can be subsonic or supersonic. This makes them more promising for measuring anisotropy.

So far shear solitons in complex plasmas have not been observed to our knowledge. The experiments on the transverse shear waves [21] demonstrated pulsed waves, however, they are unlikely to be shear solitons, because their width does not increase noticeably as the amplitude decreases, as expected for solitons. In addition, their damping length is about the width of the pulse, therefore the pulses are strongly damped, and they propagate along the Y axis which is a prohibited direction in our third-order theory. A better chance to observe shear solitons is provided for waves propagating at an angle of about 10° to one of the main axes.

The property of the solitons—to slow down as their amplitude decreases—could explain some observed features of Mach cones. Laser-excited Mach cones exhibiting distinct ''bending'' of the first cone is clearly visible in Figs. 5 and 6 of Ref. [28] at the laser scanning speed of 29.3 mm/s. Such a feature can be understood if the first cone is formed by solitons not linear waves like the other weaker cones.

Finally we propose a diagnostic method using solitons. It is well known that the longitudinal dust-lattice speed c_l is proportional to the particle charge Q and depends on the lattice parameter a/λ_D [24,28]. Measuring c_l, for example, using linear compressional waves, one can determine the constraint between Q and a/λ_D. Using solitons, one can determine not only c_l but also the soliton parameter, which provides an additional constraint (21). Thus the particle charge and the lattice parameter can be calculated independently of the measurements using ''soliton diagnostics.''

APPENDIX: KINETIC COEFFICIENTS OF A 2D-LATTICE LAYER

In this section we derive the kinetic coefficients c_l, c_{tr}, σ_l, σ_{tr}, l_l, l_{tr}, and Λ_{1-5}, which are used in the dispersion

relation (3), the nonlinear wave equations (5) for the main axes, and the nonlinear wave equations (16) for an arbitrary direction. The Taylor expansion (4) of the displacement vectors is substituted into Eqs. (1). The following calculations are routine and we omit the unnecessary details.

Let us introduce four types (α, β, γ, Δ) of sums that are used to express the kinetic coefficients:

$$S_{i,j} \equiv \{\alpha,\beta,\gamma,\Delta\}_{i,j} = \sum_{s' \neq s} \{C_\alpha, C_\beta, C_\gamma, C_\Delta\} (\delta x)^i (\delta y)^j, \tag{41}$$

where $\delta x \equiv x_{s'} - x_s$, $\delta y \equiv y_{s'} - y_s$ are the displacements introduced in Eq. (4); all the coefficients C_α, C_β, C_γ, and C_Δ are functions of $r \equiv r_{s',s} = \sqrt{(\delta x)^2 + (\delta y)^2}$, and can be written as the sequential derivatives of the interparticle interaction energy U,

$$C_\alpha = \frac{dU}{rdr}, \quad C_\beta = \frac{dC_\alpha}{rdr}, \quad C_\gamma = \frac{dC_\beta}{rdr}, \quad C_\Delta = \frac{dC_\gamma}{rdr},$$

$$U = \frac{Q^2}{r} e^{-r/\lambda_D}. \tag{42}$$

Note that for a perfect crystal (the only case we discuss here) sums $S_{i,j}$ with the odd indices are identically equal to zero. Nonzero sums with even indices obey certain symmetry relations (which are valid for all sums of the type of α, β, γ, or Δ):

$$S_{0,2} = S_{2,0}, \quad S_{0,4} = S_{4,0} = 3S_{2,2}, \quad S_{0,6} = 3S_{4,2} + 2S_{2,4},$$

$$S_{6,0} = 3S_{2,4} + 2S_{4,2}. \tag{43}$$

These relations allow us to reduce the number of sums that have to be calculated.

Using the sums (41) the phonon speed can be expressed as

$$c_l^2 = \tfrac{1}{2}(\alpha_{0,2} + \beta_{2,2}), \quad c_{tr}^2 = \tfrac{1}{2}(\alpha_{0,2} + 3\beta_{2,2}). \tag{44}$$

They are isotropic, and correspond to those shown in Fig. (2) at the wave number $ka = 0$.

The dispersion lengths obey the relations

$$c_l^2 l_l^2(\theta) = \tfrac{1}{48}[6\alpha_{2,2} + 5(\beta_{4,2} + \beta_{2,4}) + (\beta_{2,4} - \beta_{4,2})\cos(6\theta)],$$

$$\sigma_{tr}(\theta) c_{tr}^2 l_{tr}^2(\theta) = \tfrac{1}{48}[6\alpha_{2,2} + (\beta_{4,2} + \beta_{2,4}) - (\beta_{2,4} - \beta_{4,2})\cos(6\theta)], \tag{45}$$

$$\sigma_{cr}(\theta) c_{tr}^2 l_{cr}^2(\theta) = \tfrac{1}{48}(\beta_{2,4} - \beta_{4,2})\sin(6\theta),$$

where the dispersion signs $\sigma_{tr}(\theta)$, $\sigma_{cr}(\theta)$ are defined by Eqs. (17) in the main text.

The second-order coefficients of nonlinearity are such that

$$c_l^2 \Lambda_1(\theta) = \tfrac{1}{4}[6\beta_{2,2} + \gamma_{2,4} + \gamma_{2,4} - (\gamma_{2,4} - \gamma_{4,2})\cos(6\theta)],$$

$$c_l^2 \Lambda_2(\theta) = \tfrac{1}{4}[18\beta_{2,2} + 5(\gamma_{2,4} + \gamma_{2,4}) + (\gamma_{2,4} - \gamma_{4,2})\cos(6\theta)], \tag{46}$$

$$c_l^2 \Lambda_5(\theta) = \tfrac{1}{4}(\gamma_{2,4} - \gamma_{4,2})\sin(\theta).$$

The third-order coefficients of nonlinearity for the main directions of propagation satisfy the relations,

$$c_l^2 \Lambda_3^{(X)} = \tfrac{1}{2}[3\beta_{2,2} + 3(\gamma_{2,4} + \gamma_{4,2}) + \Delta_{6,2}],$$
$$c_l^2 \Lambda_3^{(Y)} = \tfrac{1}{2}[3\beta_{2,2} + 3(\gamma_{2,4} + \gamma_{4,2}) + \Delta_{2,6}], \tag{47}$$

$$c_l^2 \Lambda_4^{(X)} = \tfrac{1}{2}[9\beta_{2,2} + 3\gamma_{2,4} + 2\gamma_{4,2}],$$
$$c_l^2 \Lambda_4^{(Y)} = \tfrac{1}{2}[6\beta_{2,2} + 3\gamma_{4,2} + 2\gamma_{2,4}], \tag{48}$$

where upper indices (X), or (Y) mark the direction of the wave propagation (along X or Y axis).

The kinetic coefficients obey certain symmetry relations, which can be used to check calculations independently. Let us introduce the difference

$$\delta(F) = F^{(Y)} - F^{(X)} \tag{49}$$

between two values taken for two main directions of the wave propagation. Then it can be easily checked that the following relations are true:

$$c_l^2 \delta(l_l^2) + c_{tr}^2 \delta(l_{tr}^2) = 0, \quad \delta(\Lambda_1) + \delta(\Lambda_2) = 0,$$

$$\delta(\Lambda_2) + 3\delta(\Lambda_4) = 0. \tag{50}$$

The sums $S_{i,j}$ determine the dependence of the kinetic coefficients on the lattice parameter. Unfortunately, these sums could not be calculated analytically. Therefore we computed them numerically taking into account the interaction with 100 nearest neighbors, which should provide enough accuracy for the lattice parameters of interest. The results are shown in Figs. 3 and 4, and listed in Tables I, II, and III.

[1] J. Robinson and J. Russel, in *Report of the Committee on Waves, Reports of the 7th Meeting of the British Association for the Advancement of Science* (John Murray, London, 1838), p. 417.

[2] D. Korteweg and G. de Vries, Philos. Mag. **39**, 422 (1895).

[3] V. Petviashvili, *Reviews of Plasma Physics* (Consultants Bureau, New York, 1986), Vol. 9, pp. 59–101.

[4] H. Y. Hao and H. J. Maris, Phys. Rev. B **64**, 064302 (2001).

[5] S. Popel and M. Yu, Contrib. Plasma Phys. **35**, 103 (1995).

[6] Y. Nakamura and A. Sarma, Phys. Plasmas **8**, 3921 (2001).

[7] N. Rao, P. Shukla, and M. Yu, Planet. Space Sci. **38**, 543 (1990).

[8] A. V. Ivlev and G. Morfill, Phys. Rev. E **63**, 026412 (2001).

[9] F. Melandsø, Phys. Plasmas **3**, 3890 (1996).

[10] D. Samsonov, A. V. Ivlev, R. A. Quinn, G. Morfill, and S. Zhdanov, Phys. Rev. Lett. **88**, 095004 (2002).
[11] E. Whipple, Rep. Prog. Phys. **44**, 1197 (1981).
[12] H. Ikezi, Phys. Fluids **29**, 1764 (1986).
[13] J. H. Chu and Lin I, Phys. Rev. Lett. **72**, 4009 (1994).
[14] Y. Hayashi and K. Tachibana, Jpn. J. Appl. Phys., Part 2 **33**, L804 (1994).
[15] H. Thomas, G. E. Morfill, V. Demmel, J. Goree, B. Feuerbacher, and D. Möhlmann, Phys. Rev. Lett. **73**, 652 (1994).
[16] A. Melzer, T. Trottenberg, and A. Piel, Phys. Lett. A **191**, 301 (1994).
[17] H. Thomas and G. Morfill, Nature (London) **379**, 806 (1996).
[18] J. Maddox, Nature (London) **370**, 411 (1994).
[19] S. Vladimirov, P. Shevchenko, and N. Cramer, Phys. Plasmas **5**, 4 (1998).
[20] A. Homann, A. Melzer, R. Madani, and A. Piel, Phys. Lett. A **173**, 242 (1998).
[21] S. Nunomura, D. Samsonov, and J. Goree, Phys. Rev. Lett. **84**, 5141 (2000).
[22] D. Samsonov, J. Goree, Z. W. Ma, A. Bhattacharjee, H. M. Thomas, and G. E. Morfill, Phys. Rev. Lett. **83**, 3649 (1999).
[23] D. Samsonov, J. Goree, H. M. Thomas, and G. E. Morfill, Phys. Rev. E **61**, 5557 (2000).
[24] F. M. Peeters and X. Wu, Phys. Rev. A **35**, 3109 (1987).
[25] D. H. E. Dubin, Phys. Plasmas **7**, 3895 (2000).
[26] U. Konopka, L. Ratke, and H. M. Thomas, Phys. Rev. Lett. **79**, 1269 (1997).
[27] U. Konopka, G. E. Morfill, and L. Ratke, Phys. Rev. Lett. **84**, 891 (2000).
[28] A. Melzer, S. Nunomura, D. Samsonov, Z. W. Ma, and J. Goree, Phys. Rev. E **62**, 4162 (2000).
[29] M. J. Lighthill, Proc. R. Soc. London, Ser. A **299**, 28 (1967).
[30] M. Ablowitz and H. Segur, *Solitons and the Inverse Scattering Transform* (SIAM, Philadelphia, 1981).
[31] B. B. Kadomtsev, *Collective Phenomena in Plasmas* (Nauka, Moscow, 1976).